A statistical mechanical model for inverse melting

Melissa R. Feeney and Pablo G. Debenedetti[a)]
Department of Chemical Engineering, Princeton University, Princeton, New Jersey 08544

Frank H. Stillinger
Department of Chemistry, Princeton University, Princeton, New Jersey 08544

(Received 14 April 2003; accepted 29 May 2003)

Inverse melting is the situation in which a liquid freezes when it is heated isobarically. Both helium isotopes exhibit intervals of inverse melting at low temperature, and published data suggests that isotactic poly (4-methylpentene-1) also displays this unusual phase behavior. Here we propose a statistical mechanical model for inverse melting. It is a decorated modification of the Gaussian core model, in which particles possess a spectrum of thermally activated internal states. Excitation leads to a change in a particle's Gaussian interaction parameters, and this can result in a spatially periodic crystal possessing a higher entropy than the fluid with which it coexists. Numerical solution of the model, using integral equations and the hypernetted chain closure for the fluid phase, and the Einstein model for the solid phases, identifies two types of inverse melting. One mimics the behavior of the helium isotopes, for which the higher-entropy crystal is denser than the liquid. The other corresponds to inverse melting in poly(4-methylpentene-1), where the high-entropy crystal is less dense than the liquid with which it coexists. © *2003 American Institute of Physics.*
[DOI: 10.1063/1.1593018]

I. INTRODUCTION

First-order melting/freezing transitions between spatially periodic crystals and isotropic liquid phases of pure substances have scientific and technological implications whose significance is hard to overestimate. Crystal structures and their melting temperatures reveal detailed characteristics of atomic and molecular interactions.[1] The transition itself forms the basis of the zone-refining method for purification.[2] The ability to circumvent crystal nucleation and growth during liquid supercooling is a key to forming many amorphous materials.[3] And of course the capacity to produce nearly perfect semiconducting single crystals enables much of modern electronic technology.[4]

The most common melting scenario under constant pressure (isobaric) conditions entails positive increments for both molar volume and molar entropy,

$$\Delta v = v^{(\mathrm{liq})} - v^{(\mathrm{cr})} > 0,$$
$$\Delta s = s^{(\mathrm{liq})} - s^{(\mathrm{cr})} > 0. \tag{1.1}$$

Somewhat less common are those cases in which Δs remains positive, but $\Delta v < 0$, i.e., the liquid is more dense than the crystal from which it is formed. The most familiar example of this latter category, at ambient pressure, is water; elements exhibiting the same behavior are silicon, gallium, antimony, and bismuth.[5]

The present paper is devoted to a third type of melting scenario, for which the entropy change Δs is negative, and Δv can have either sign. This counterintuitive situation, which involves equilibrium freezing of the liquid as a result of isobaric heating, has been called ''inverse melting.''[6,7] The crystal phase that coexists with the liquid at an inverse-melting point has higher molar entropy than that liquid, the reverse of the usual situation. Both helium isotopes ^{3}He and ^{4}He at low temperature exhibit intervals of inverse melting.[8,9] In addition, reports have been published indicating that the polymeric substance isotactic poly (4-methylpentene-1), ''P4MP1,'' also exhibits inverse melting.[10]

To the best of our knowledge, no general microscopic theory or model has yet been proposed to describe inverse melting in the domain of classical statistical mechanics. Beyond the intrinsic desire to understand the reasons underlying this fascinating phenomenon, the development of relevant theory and/or well-defined models might have as a by-product suggestions for synthesis of new materials exhibiting inverse melting. Here we propose and investigate a classical statistical model that displays a range of inverse melting phenomena. This model is an internally decorated version of the so-called Gaussian core model (GCM).[11–14]

In order to provide a clear basis for discussing our inverse melting model, and to make this presentation as nearly self-contained as practicable, Sec. II reviews several fundamental and relevant thermodynamic identities. This is followed in Sec. III by a brief definition and description of the original undecorated GCM. Section IV introduces the extended Gaussian core model (EGCM), motivated by simple arguments about the necessity of coupling intramolecular degrees of freedom to intermolecular interactions in order to create an inverse melting scenario. Section V presents our approximate, but we believe reliable, method for evaluating free energies of the EGCM, required to locate melting transition curves. Numerical examples showing a diversity of inverse melting results appear in Sec. VI. Our conclusions,

a)Author to whom correspondence should be addressed. Electronic mail: pdebene@princeton.edu

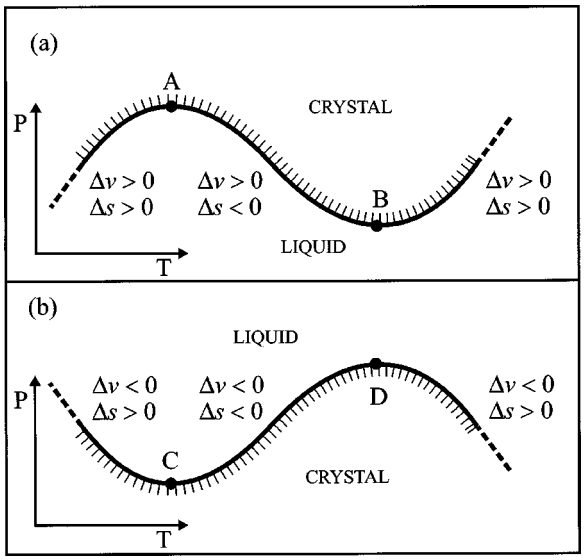

FIG. 1. The two inverse melting scenarios. The solid line is the melting curve, and the crystal phase is stable inside the hatched region. (a) $\Delta v > 0$; (b) $\Delta v < 0$. At the extrema A, B, C, and D, $\Delta s = 0$. The inverse melting intervals are AB, and CD, respectively.

and discussion of desirable directions for future study of inverse melting phenomena, form the basis of the final Sec. VII.

II. THERMODYNAMIC RELATIONS

A first-order melting/freezing transition in the temperature-pressure plane is located by the transition curve $T_m(p)$, representing the absolute melting/freezing temperature as a function of the pressure. This transition can equally well be represented by the inverse function $p_m(T)$, the melting/freezing pressure at any given absolute temperature. The most basic thermodynamic identity satisfied by the transition locus is the Clausius–Clapeyron equation, describing its slope,[15]

$$dP_m(T)/dT = \Delta s/\Delta v, \tag{2.1}$$

where Δs and Δv were defined above in Eq. (1.1).

Two inverse melting categories can be distinguished, depending on the sign of the molar volume change Δv. These are illustrated schematically in Figs. 1(a) and 1(b). The case 1(a), with inverse melting interval AB, involves opposite signs for the numerator and the denominator in the Clausius–Clapeyron right-hand member, so the slope of the melting curve is negative between A and B. The case 1(b), with inverse melting interval CD, involves negative signs for both the numerator and the denominator in the Clausius–Clapeyron right-hand member, so the slope of the melting curve is positive between C and D.

The zero-slope points A, B, C, and D in Figs. 1(a) and 1(b) are positions along the melting curves at which Δs vanishes, as it continuously changes from positive to negative, or the reverse. Because $\Delta s = 0$ at these extrema, it has been suggested that such points should be called "Kauzmann points," on account of their thermodynamic kinship to similar vanishing-entropy points that play a role in the theory of glass transitions.[3]

The first-order differential characterization of the transition curve provided by the Clausius–Clapeyron equation can be extended to the second derivative, i.e., the curvature. The result is especially simple at the extremal points of vanishing slope (A,B,C,D). At any one of these special points one finds[7]

$$\frac{d^2P_m(T)}{dT^2} = \frac{c_p^{(\mathrm{liq})} - c_p^{(\mathrm{cr})}}{T(v^{(\mathrm{liq})} - v^{(\mathrm{cr})})}, \tag{2.2}$$

where the numerator of the right member involves the difference of constant-pressure molar heat capacities for the two phases at that extremal coexistence point. In conjunction with Fig. 1, this latter identity establishes the following relative magnitudes of the heat capacities at the four extremal points:

$$\begin{aligned} &c_p^{(\mathrm{cr})} > c_p^{(\mathrm{liq})} > 0 \quad (\text{at A,C}), \\ &c_p^{(\mathrm{liq})} > c_p^{(\mathrm{cr})} > 0 \quad (\text{at B,D}). \end{aligned} \tag{2.3}$$

The extremal (Kauzmann) points A, B, C, D on a phase transition curve, at which the molar entropy change Δs vanishes, perforce are points at which the molar enthalpy change Δh also vanishes,

$$\Delta h = h^{(\mathrm{liq})} - h^{(\mathrm{cr})} \equiv T\Delta s. \tag{2.4}$$

By considering the variations in thermodynamic properties for both liquid and crystal phases at positions in the T,P-plane displaced from the extremal points, it is possible to derive expressions for the slopes of curves along which, respectively, Δs and Δh continue to vanish,[7]

$$\left(\frac{dP}{dT}\right)_{\Delta h = 0} = \frac{c_p^{(\mathrm{liq})} - c_p^{(\mathrm{cr})}}{v^{(\mathrm{liq})}(1 - T\alpha^{(\mathrm{liq})}) - v^{(\mathrm{cr})}(1 - T\alpha^{(\mathrm{cr})})}; \tag{2.5}$$

$$\left(\frac{dP}{dT}\right)_{\Delta s = 0} = \frac{c_p^{(\mathrm{liq})} - c_p^{(\mathrm{cr})}}{T[\,\alpha^{(\mathrm{liq})} v^{(\mathrm{liq})} - \alpha^{(\mathrm{cr})} v^{(\mathrm{cr})}\,]}. \tag{2.6}$$

Here, the α's stand for isobaric thermal expansion coefficients of the two phases. The curves for which these expressions give the slopes are coincident only at the extremal points of $P_m(T)$. As a generalization of the aforementioned Kauzmann point, a $\Delta s = 0$ curve described by Eq. (2.6) can be called a "Kauzmann curve." Although Eq. (2.6) is formally identical to the first Ehrenfest relation for a line of second-order phase transitions,[16] its meaning is fundamentally different in the present context.

It is useful to derive the criteria that determine the sign of the slope of Kauzmann curves at points A, B, C, and D (Fig. 1). Taking into account inequality (2.3) and Eq. (2.6), the possible cases are given in Table I.

III. REVIEW OF STANDARD GCM

The standard GCM is a classical many-body model consisting of N particles whose interaction potential, when those particles have positions $\mathbf{r}_1 \cdots \mathbf{r}_N$, has the following pairwise additive form:[11]

TABLE I. Criteria for the sign of the slope of the Kauzmann curve at the melting curve extrema.

$\alpha^{(\mathrm{liq})}$	$\alpha^{(\mathrm{cr})}$	$dP_K/dT>0$[a]	$dP_K/dT<0$[a]
		B(+), D(−)[b]	
>0	>0	$\alpha^{(\mathrm{cr})}/\alpha^{(\mathrm{liq})}<1\pm\delta$	$\alpha^{(\mathrm{cr})}/\alpha^{(\mathrm{liq})}>1\pm\delta$
>0	<0	always	never
<0	>0	never	always
<0	<0	$\lvert\alpha^{(\mathrm{cr})}\rvert/\lvert\alpha^{(\mathrm{liq})}\rvert>1\pm\delta$	$\lvert\alpha^{(\mathrm{cr})}\rvert/\lvert\alpha^{(\mathrm{liq})}\rvert<1\pm\delta$
		A(+), C(−)[b]	
>0	>0	$\alpha^{(\mathrm{cr})}/\alpha^{(\mathrm{liq})}>1\pm\delta$	$\alpha^{(\mathrm{cr})}/\alpha^{(\mathrm{liq})}<1\pm\delta$
>0	<0	never	always
<0	>0	always	never
<0	<0	$\lvert\alpha^{(\mathrm{cr})}\rvert/\lvert\alpha^{(\mathrm{liq})}\rvert<1\pm\delta$	$\lvert\alpha^{(\mathrm{cr})}\rvert/\lvert\alpha^{(\mathrm{liq})}\rvert>1\pm\delta$

[a]P_K is the pressure along the Kauzmann curve. Equation (2.6) gives dP_K/dT.

[b]Coexisting liquid and crystal volumes are related by $v^{(\mathrm{liq})}=v^{(\mathrm{cr})}(1\pm\delta)$, where $\delta>0$. The + sign applies at A and B ($\Delta v>0$), and the − sign applies at C and D ($\Delta v<0$).

$$\Phi(\mathbf{r}_1\cdots\mathbf{r}_N)=\epsilon\sum_{i<j}\exp[-(r_{ij}/\sigma)^2]\quad(\epsilon,\sigma>0). \tag{3.1}$$

Although the usual procedure in analyzing the statistical mechanics of this model is to choose energy and length scales so that both ϵ and σ are equal to unity,[11–14] we retain them as explicit parameters to lead naturally into the extension developed in the following Sec. IV.

The N particles of the GCM nominally are spherically symmetric and structureless. However, it has been established that the effective interactions that operate between complex molecules and their aggregates in suitable solvents can be close to repelling Gaussian functions of interparticle separation, consistent with the form shown in Eq. (3.1). This correspondence includes solutions of linear polymers,[13,17] highly branched "star" polymers,[18] and colloidal particles.[19]

A combination of analytical[11,13,20] and simulation[12,21] studies have reached consensus on the phase behavior of the standard GCM. Three distinct phases appear. At low reduced temperature k_BT/ϵ (where k_B is Boltzmann's constant), and relatively low reduced number density $\rho\sigma^3$, the model exhibits a face-centered cubic (fcc) crystal phase. Increasing $\rho\sigma^3$ at low reduced temperature causes a first-order phase change to a body-centered cubic (bcc) crystal. At sufficiently high temperature, for any density, the model exists in an isotropic fluid phase.

Figure 2 presents the GCM phase diagram in the density–temperature and temperature–pressure planes. The most noteworthy feature exhibited by Fig. 2 is the melting-temperature maximum for the bcc crystal phase. At this maximum, the molar volumes of the coexisting crystal and fluid phases are equal. This represents the position of sign change for Δv, which is positive at lower density and pressure, and negative at higher density and pressure. However, Δs for the melting process, whether fcc or bcc crystals are involved, is always positive, i.e., no inverse melting appears for the standard GCM.

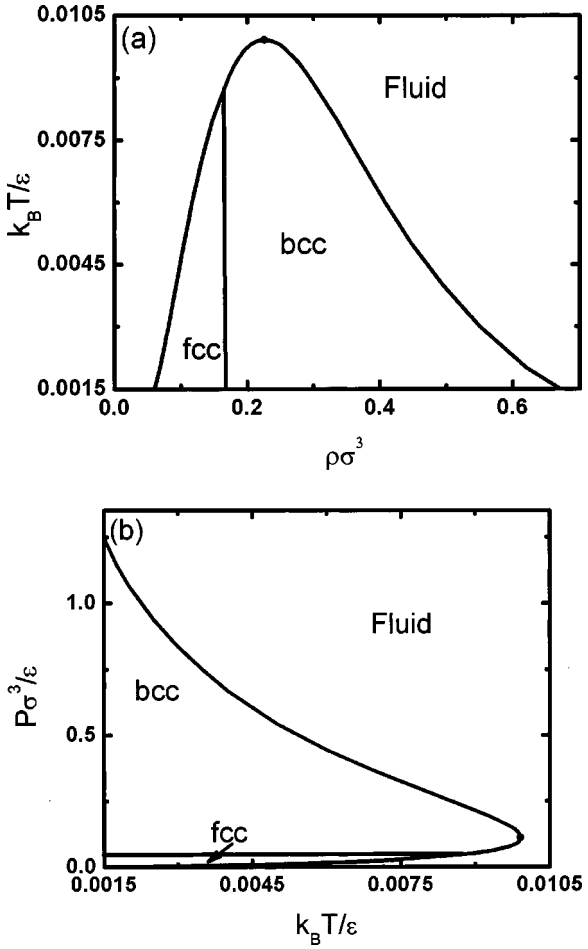

FIG. 2. Calculated phase behavior for the conventional Gaussian core model (GCM). The Ornstein–Zernike equation with hypernetted chain closure was used for the fluid phase, and the Einstein model was adopted for the solid phases. (a) Temperature–density projection. The density difference between coexisting phases is too small to be visible on the scale of the figure. (b) Pressure–temperature projection.

IV. EXTENDED GCM

In order to devise a classical statistical mechanical model that exhibits inverse melting, a mechanism must be present to cause the fluid phase at coexistence to possess lower entropy than the crystal. Such a scenario can be produced by invoking additional particle degrees of freedom beyond the center of mass positions $\mathbf{r}_1\cdots\mathbf{r}_N$. We now propose to extend the standard GCM by endowing each particle with a spectrum of internal states whose presence influences the system's potential energy function Φ. This can be implemented in such a way that the resulting extended Gaussian core model (EGCM) has the capacity to display inverse melting of either type illustrated earlier in Fig. 1.

For the task at hand it suffices to postulate a very simple discrete spectrum of internal states. In particular, we suppose that each particle in isolation possesses a nondegenerate ground state (at zero energy), and a group of $E\gg1$ degenerate and indistinguishable excited states. This latter group lies above the ground state by an excitation energy to be denoted by Δ. For accounting purposes, it will be useful to describe the internal excitation state of each particle $1\leqslant i\leqslant N$ by a discrete variable μ_i; this variable will equal 0 if particle i is

in its internal ground state, and will equal 1 if it is in any of the E internal excited states. When any one of the N particles is isolated, the probability x_1 that it is internally excited has the following form:

$$x_1=\langle \mu_i\rangle=[E^{-1}\exp(\beta\Delta)+1]^{-1}, \tag{4.1}$$

where $\beta=1/k_BT$ is the inverse temperature. The corresponding entropy per particle due to the internal degrees of freedom is

$$S^{(\mathrm{int})}/Nk_B=-(1-x_1)\ln(1-x_1)-x_1\ln(x_1/E). \tag{4.2}$$

This entropy varies between 0 at absolute zero temperature, and $k_B\ln(E+1)$ at infinite temperature. It is easy to see from Eq. (4.1) that x_1 is a monotonically decreasing function of β. This independent-particle excitation probability reaches the value 1/2 (i.e., equal chance for ground state, as for excited states) when

$$\beta_{1/2}=\Delta^{-1}\ln E. \tag{4.3}$$

Increasing both Δ and E so as to keep this last ratio fixed has the effect of narrowing the excitation transition. This sharpening can be measured by the rate of change of x_1 at the halfway point,

$$\left(\frac{dx_1}{d\beta}\right)_{\beta_{1/2}}=-\frac{\Delta}{4}. \tag{4.4}$$

In order to produce an inverse-melting scenario, the internal degrees of freedom need to interact with the centroid positions of the particles in such a way that a spatially periodic crystal phase can have greater molar entropy than the liquid with which it thermodynamically coexists. Our approach has been to postulate that the Gaussian interaction parameters ϵ, σ depend on the excitation variables μ_i, while otherwise retaining the form, Eq. (3.1), of the many-body interaction potential. Thus we write

$$\Phi(\mathbf{r}_1\cdots\mathbf{r}_N,\mu_1\cdots\mu_N)$$

$$=\sum_{i<j}\epsilon(\mu_i,\mu_j)\exp\{-[r_{ij}/\sigma(\mu_i,\mu_j)]^2\}. \tag{4.5}$$

This kind of presumption is at least somewhat realistic, in view of experimental observations of size changes of polymer coils that induce fcc to bcc ordering changes.[22]

A basic quantity of interest, especially for the study of equilibrium phase changes, is the canonical partition function $Q(N,V,T)$. It gives the Helmholtz free energy F as a function of number density and temperature,

$$Q=\exp(-\beta F) \tag{4.6}$$

from which all other thermodynamic properties can be obtained in turn. A straightforward analysis of the EGCM as postulated leads to the following expression:

$$Q=[\Gamma(\beta)]^N\sum_{n_1=0}^{N}\left[\frac{E^{n_1}\exp(-\beta\Delta n_1)}{n_1!(N-n_1)!}\right]Y(\beta,n_1), \tag{4.7}$$

where we have collected all equal contributions representing the same total number $0\leqslant n_1\leqslant N$ of internally excited particles,

$$n_1=\sum_{i=1}^{N}\mu_i. \tag{4.8}$$

The factors $\Gamma(\beta)$, one for each particle, arise from integrations over conjugate momenta; they are necessary to render Q dimensionless, but play no role in determining phase equilibria and can subsequently be disregarded. Configurational integrals for the N-body system with a fixed number n_1 of internal excitations have been denoted by $Y(\beta,n_1)$ in expression (4.7) above. The detailed form of these latter quantities is the following:

$$\begin{aligned}Y(\beta,n_1)=\int d\mathbf{r}_1\cdots\int d\mathbf{r}_N\exp\Bigg\{&-\beta\epsilon_{00}\\&\times\sum_{i=1}^{N-n_1-1}\sum_{j=i+1}^{N-n_1}\exp[-(r_{ij}/\sigma_{00})^2]\\&-\beta\epsilon_{01}\sum_{i=1}^{N-n_1}\sum_{j=N-n_1+1}^{N}\exp[-(r_{ij}/\sigma_{01})^2]\\&-\beta\epsilon_{11}\sum_{i=N-n_1+1}^{N-1}\sum_{j=i+1}^{N}\exp[-(r_{ij}/\sigma_{11})^2]\Bigg\}.\end{aligned} \tag{4.9}$$

For notational simplicity we have used 0,1 subscripts on the ϵ, σ parameters to indicate the excitation state of the particle pair involved. If all the values of ϵ's and σ's were, respectively, equal to one another, $Y(\beta,n_1)$ would be independent of n_1 and would correspond to the Helmholtz free energy excess of the unaltered GCM at β. In order to account for variations in ϵ and σ we introduce a mean pair of values $\epsilon_{\mathrm{av}}(n_1)$ and $\sigma_{\mathrm{av}}(n_1)$. $Y(\beta,n_1)$ can then be decomposed into two contributions,

$$\begin{aligned}Y(\beta,n_1)=V^N\exp\{-N[&\beta f_{\mathrm{GCM}}(\beta\epsilon_{\mathrm{av}},\rho\sigma_{\mathrm{av}}^3(n_1))\\&+\beta f_{\mathrm{corr}}(\beta\epsilon_{\mathrm{corr}},\rho\sigma_{\mathrm{corr}}^3(n_1))]\}.\end{aligned} \tag{4.10}$$

Here f_{GCM} is the excess Helmholtz free energy per particle of the uniform GCM at the ϵ_{av} and σ_{av}, and f_{corr} is a correction term to the free energy that accounts for deviations in σ and ϵ from their mean values. For any given value of n_1 it may be possible to choose ϵ_{av} and σ_{av} so that the correction vanishes. Considering only linear corrections for simplicity, the configurational free energy for the parameter-varied GCM must have the following form:

$$Nf_{\mathrm{GCM}}(\beta\epsilon,\rho\sigma^3)+\sum_{i<j}[A(\beta\epsilon,\rho\sigma^3)\delta\sigma_{ij}+B(\beta\epsilon,\rho\sigma^3)\delta\epsilon_{ij}]. \tag{4.11}$$

The coefficients A and B can be identified, respectively, by changing all σ's together, or all ϵ's together,

$$\begin{aligned}A(\beta\epsilon,\rho\sigma^3)&=\frac{6\rho\sigma^2}{N-1}\frac{\partial(f_{\mathrm{GCM}})}{\partial(\rho\sigma^3)},\\B(\beta\epsilon,\rho\sigma^3)&=\frac{2\beta}{N-1}\frac{\partial(f_{\mathrm{GCM}})}{\partial(\beta\epsilon)}.\end{aligned} \tag{4.12}$$

Applying these formal linear correction results to the excited polymer case, the configurational free energy will be determined by

$$\ln\left(\frac{V^N}{Y(\beta,n_1)}\right)=N\beta\Bigg\{f_{\mathrm{GCM}}[\beta\epsilon_{\mathrm{av}},\rho\sigma_{\mathrm{av}}^3(n_1)]+3\rho\sigma_{\mathrm{av}}^2(n_1)\frac{\partial f}{\partial(\rho\sigma^3)}\Bigg[\left(1-\frac{n_1}{N}\right)^2(\sigma_{00}-\sigma_{\mathrm{av}}(n_1))+\left(\frac{2n_1}{N}\right)\left(1-\frac{n_1}{N}\right)(\sigma_{01}-\sigma_{\mathrm{av}}(n_1))+\left(\frac{n_1}{N}\right)^2(\sigma_{11}-\sigma_{\mathrm{av}}(n_1))\Bigg]+\beta\frac{\partial f}{\partial(\beta\epsilon)}\Bigg[\left(1-\frac{n_1}{N}\right)^2(\epsilon_{00}-\epsilon_{\mathrm{av}}(n_1))+\frac{2n_1}{N}\left(1-\frac{n_1}{N}\right)(\epsilon_{01}-\epsilon_{\mathrm{av}}(n_1))+\left(\frac{n_1}{N}\right)^2(\epsilon_{11}-\epsilon_{\mathrm{av}}(n_1))\Bigg]\Bigg\}. \tag{4.13}$$

Therefore the linear corrections vanish if one chooses

$$\sigma_{\mathrm{av}}(n_1)=\left(1-\frac{n_1}{N}\right)^2\sigma_{00}+\frac{2n_1}{N}\left(1-\frac{n_1}{N}\right)\sigma_{01}+\left(\frac{n_1}{N}\right)^2\sigma_{11}, \tag{4.14}$$

$$\epsilon_{\mathrm{av}}(n_1)=\left(1-\frac{n_1}{N}\right)^2\epsilon_{00}+\frac{2n_1}{N}\left(1-\frac{n_1}{N}\right)\epsilon_{01}+\left(\frac{n_1}{N}\right)^2\epsilon_{11}.$$

By making this choice, the canonical partition function simplifies to the following:

$$Q=[\Gamma(\beta)]^N\sum_{n_1=0}^{N}\left[\frac{E^{n_1}\exp(-\beta\Delta n_1)}{n_1!(N-n_1)!}\right]\times\exp(-N\beta f_{\mathrm{GCM}}[\beta\epsilon_{\mathrm{av}}(n_1),\rho\sigma_{\mathrm{av}}^3(n_1)]). \tag{4.15}$$

In the thermodynamic limit, the sum on the right-hand side of Eq. (4.15) can be replaced by its maximum term. However, in order to evaluate Eq. (4.15) an expression for f_{GCM}, the excess Helmholtz free energy of the unaltered GCM, is needed for both the fluid and solid phases.

The extended GCM with $E=1$ corresponds to a binary GCM, but with temperature-dependent composition. Important aspects of the binary GCM have been investigated recently, including fluid–fluid separation[23] and wetting.[24] Over the range of parameters studied in this work, no fluid–fluid transition is predicted to occur. It is possible that a pronounced nonadditivity of particle diameters ($\sigma_{12}\gg\sigma_{11},\sigma_{22}$) may destabilize the fluid phase and cause separation. This will be investigated in future work.

V. FREE ENERGY OF THE GCM

This section outlines the procedure for calculating the Helmholtz free energies of the respective phases in the GCM. For the fluid phase, integral equations are adopted. For the solid phases the Einstein model is implemented.

A. Fluid phase

The quantity of interest is the radial distribution function, $g(r)$. The starting point for the calculation of $g(r)$ is the Ornstein–Zernike (OZ) equation,

$$h(r_{12})=c(r_{12})+\rho\int c(r_{13})h(r_{23})d\mathbf{r}_3, \tag{5.1}$$

where $h(r)=g(r)-1$, and $c(r)$ is the direct correlation function. The OZ equation is, in effect, the definition of the direct correlation function.[25] As this equation relates two unknown functions, $g(r)$ and $c(r)$, one more relation or closure is needed to determine $c(r)$ and $h(r)$. The hypernetted-chain (HNC) equation, which we adopt in this work, provides an approximate relationship between $h(r)$ and $c(r)$. It is given by

$$c(r)=-\beta\phi(r)+h(r)-\ln[1+h(r)], \tag{5.2}$$

where $\phi(r)$ is the pair potential.[25] A recent theoretical and computational investigation of the GCM reported that the HNC closure is reliable in predicting structure in the fluid phase over a large range of densities and temperatures.[13] All of the thermodynamic quantities can be calculated once the radial distribution function has been determined as a function of T and ρ. The virial pressure equation provides a relationship between the radial distribution function and the excess pressure,

$$P_{\mathrm{ex}}=P-\rho k_BT=-\frac{2\pi\rho^2}{3}\int_0^\infty r^3\phi'(r)g(r)dr, \tag{5.3}$$

where[25] $\phi'(r)=d\phi(r)/dr$. The excess Helmholtz free energy can be determined by integrating the thermodynamic relation $P_{\mathrm{ex}}=-\partial F_{\mathrm{ex}}/\partial V$ from $\rho=0$ up to the given density, under the initial condition $F_{\mathrm{ex}}(\rho=0,T)=0$. The Helmholtz free energy is given by the sum of the ideal and excess terms,

$$\frac{F^{\mathrm{liquid}}(\rho,T)}{Nk_BT}=\ln\left(\frac{\rho\Lambda^3}{e}\right)+\frac{F_{\mathrm{ex}}(\rho,T)}{Nk_BT}, \tag{5.4}$$

where Λ is the de Broglie wavelength for the structureless GCM particles.

B. Solid phase

In order to calculate the free energies of the unaltered GCM a theory is needed for the candidate crystalline states of the model. Because the GCM is a soft interaction pair potential, a harmonic approximation in the solid is justified and the simple Einstein model is adopted. The Einstein model approximates the crystal as $3N$ independent harmonic oscillators.[26] All the molecules are assumed to vibrate at one frequency, the Einstein frequency (ω_E), about their equilibrium positions. The Einstein frequency is a measure of the restoring force on a single particle due to the cage of neighboring particles. The Einstein frequency is proportional the trace of Hessian matrix. The Hessian matrix is calculated numerically by summing the second derivative of the pair potential over all neighbors with respect to a single central

particle. The Helmholtz free energy of the Einstein solid in the high-temperature classical limit is given by

$$F^{\text{solid}} = U_0 + 3Nk_BT \ln\left(\frac{\hbar\omega_E}{k_BT}\right), \tag{5.5}$$

where U_0 is the potential energy and $\hbar$ is Planck's constant divided by 2π.

With expressions for the free energies of the solid and fluid phases of the GCM, Eq. (5.4) and Eq. (5.5), respectively, it is now possible to calculate phase equilibrium for the EGCM by Eqs. (4.14) and (4.15). In the thermodynamic limit only the maximum term of Eq. (4.15) is significant; it determines the fraction of excited particles, n_1/N, as a function of ρ and β. In general, two internal consistency conditions arise: one for σ_{av} and one for ϵ_{av}, Eq. (4.14). If all of the particles in the solid and fluid phases are excited, $n_{1,S}/N \cong 1$ and $n_{1,F}/N \cong 1$, respectively, over the range of temperatures and densities of interest, Eq. (4.14) shows that $\sigma_{\text{av}} = \sigma_{11}$ and $\epsilon_{\text{av}} = \epsilon_{11}$. Therefore the phase behavior predicted by the EGCM is identical to that determined by the GCM with $\epsilon = \epsilon_{11}$, $\sigma = \sigma_{11}$. Alternately, if $n_{1,F}/N \cong n_{1,S}/N \cong 0$ over the density and temperature range of interest, the EGCM and the GCM with $\epsilon = \epsilon_{00}$, $\sigma = \sigma_{00}$ will predict equivalent phase behavior.

VI. NUMERICAL EXAMPLES

This section presents phase diagrams for the EGCM in which n_1 varies with temperature and density in the range of interest. The EGCM has eight parameters which can be varied independently $(E, \Delta, \epsilon_{00}, \epsilon_{01}, \epsilon_{11}, \sigma_{00}, \sigma_{01}, \sigma_{11})$. To simplify calculations, the energy parameters were set equal to one another $(\epsilon_{00} = \epsilon_{01} = \epsilon_{11} = \epsilon)$. The interparticle diameters were varied within physically intuitive constraints, e.g., $(\sigma_{00} < \sigma_{01} < \sigma_{11}$ or $\sigma_{00} > \sigma_{01} > \sigma_{11})$. Three phases are considered: fluid, bcc solid, and fcc solid. For clarity we have omitted the solid–solid equilibrium lines in the phase diagrams shown in this section. For every case considered we use the more stable crystal form at a particular temperature and pressure. Usually this is the bcc crystal; the fcc crystal is the stable phase at low pressures, as in the GCM (see Fig. 2).

Figure 3 shows the solid–fluid equilibrium predicted by the EGCM with $\sigma_{01}/\sigma_{00} = 0.8$, $\sigma_{11}/\sigma_{00} = 0.7$, $\Delta/\epsilon = 25$, and $E = \exp(250)$. The salient feature of Fig. 3 is the large region in which the fluid crystallizes upon isobaric heating (segment of the melting curve joining points a and b). This result is quite significant, since to the best of our knowledge no general classical microscopic theory or model has captured the molecular mechanisms sufficient to produce inverse melting. The anomalous region occurs along the upper pressure branch of the melting curve, where the volume of melting is negative. The region of inverse melting is bounded by the extrema in the melting pressure–temperature curve. The fractions of excited particles in the fluid and solid phases, $x_F = n_{1,F}/N$, $x_S = n_{1,S}/N$, along the melting curve are shown in Fig. 4. The difference between the fraction of excited particles in solid and fluid phases is also shown. The vertical line Fig. 4(a) corresponds to the upper melting temperature T_u associated with the corresponding pressure P_u [point 3 in

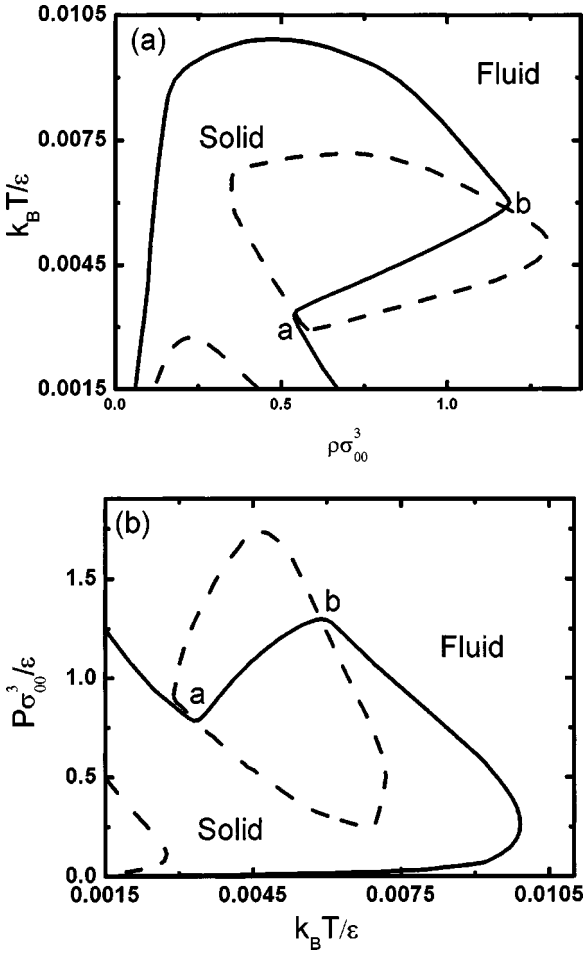

FIG. 3. Calculated phase behavior for the extended Gaussian core model (EGCM) showing inverse melting interval ab on the high-pressure branch of the solid–liquid equilibrium curve. The model parameters are $\sigma_{01}/\sigma_{00} = 0.8$, $\sigma_{11}/\sigma_{00} = 0.7$, $\Delta/\epsilon = 25$, and $E = \exp(250)$. Coexistence curves (dark line) and Kauzmann equal-entropy curves (dashed lines) are shown. (a) Temperature–density projection. The density difference between coexisting phases is too small to be visible on the scale of the figure. (b) Pressure–temperature projection. Solid–solid equilibrium lines are omitted for clarity. Calculations are shown for the more stable crystal phase at any given temperature and pressure.

Fig. 4(b)]. Points to the left of the vertical line correspond to the fraction of excited particles along the low-pressure branch of the melting curve $(P < P_u)$, while points to the right of the vertical line correspond to the fraction of particles excited along the high-pressure branch $(P > P_u)$. At low temperatures and pressures, the fraction of excited particles is vanishingly small, $x_F \cong x_S \cong 0$. At the upper melting/freezing temperature, point 3, the fraction of particles excited is nonzero and is greater in the fluid than in the solid phase. Upon following the coexistence curve to higher pressures, the overwhelming majority of the particles in both phases are excited, $x_F \cong x_S \cong 1$. At the maximum freezing/melting pressure, point 2, the fraction of particles excited has begun to decrease. Points 1 and 2 bound the region of inverse melting. The fraction of excited particles in this region decreases as the temperature is lowered. It is important to note that in this region, the fraction of excited particles in the solid phase is always greater than the corresponding fraction in the fluid phase. This is consistent with the thermodynamic restriction

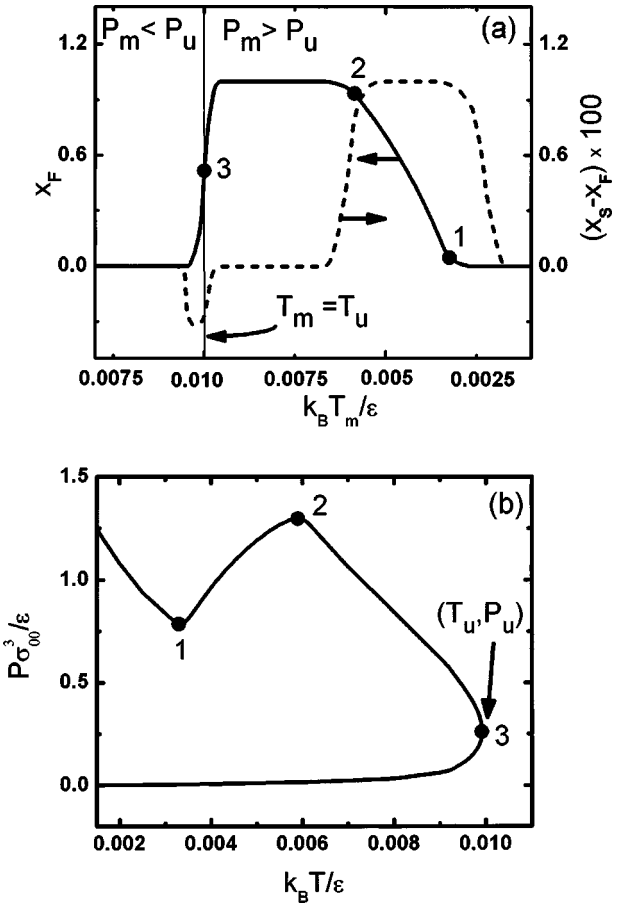

FIG. 4. (a) The fraction of excited particles in the fluid phase, x_F (solid line) and the difference between the fraction of excited particles in the solid and fluid phases (dashed line) along the melting curve. The vertical line corresponds to the upper melting temperature, T_u; values of the melting temperature decrease to the right and left of this line (i.e., the melting curve is "unfolded" along the x-axis). Points to the left of the vertical line correspond to the lower pressure branch ($P_m < P_u$) and points to the right correspond to the upper pressure branch ($P_m > P_u$). Points 1 and 2 bound the region of inverse melting. Point 3 corresponds to the upper melting temperature T_u and its corresponding pressure, P_u. EGCM model parameters as in Fig. 3. (b) Pressure–temperature projection of the calculated melting curve.

that inverse melting occurs only when the entropy of the solid is greater than that of the fluid.

Under conditions where $x_F \cong x_S \cong 0$ or $x_S \cong x_F \cong 1$, the phase behavior predicted by the EGCM is the same as that of the GCM, with $\sigma_{\mathrm{av}} = \sigma_{00}$ and $\epsilon_{\mathrm{av}} = \epsilon_{00}$, or with $\sigma_{\mathrm{av}} = \sigma_{11}$ and $\epsilon_{\mathrm{av}} = \epsilon_{11}$, respectively. Recognizing that pressure scales as energy over volume it follows that decreasing the characteristic length scale, σ, results in increasing pressure. It thus becomes possible to understand why the EGCM with $\sigma_{00} > \sigma_{11}$ and values of x_F and x_S shown in Fig. 4(a) predicts inverse melting. A closer look at x_F and x_S along the high-pressure branch of the melting curve reveals that $x_F \cong x_S \cong 1$ for $0.0098 \geqslant T_m^* \geqslant 0.0070$ and that $x_F \cong x_S \cong 0$ for $T_m^* \leqslant 0.0018$ ($T^* = k_B T/\epsilon$). Therefore if the ratio of σ_{00} to σ_{11} is large enough, the pressure at point $2[P_2 \sigma_{00}^3/\epsilon \cong P_{\mathrm{GCM}}^* (\sigma_{00}/\sigma_{11})^3]$ will be greater than at point $1[P_1 \sigma_{00}^3/\epsilon \approx P_{\mathrm{GCM}}^*]$, which is the case as seen in Fig. 4(b) ($P^* = P\sigma_{00}^3/\epsilon$). The range of pressures over which the EGCM model predicts inverse melting diminishes as the ratio of σ_{00} to σ_{11} is decreased. The values of Δ and E affect the temperature range in which inverse melting is predicted. While E is quite large in the case shown in Fig. 3, it is a reasonable estimate for the number of internal degrees of freedom in a polymer chain. For example, a polymer chain with 250 monomer units, each exhibiting 3 degrees of freedom, has approximately 3^{250} internal degrees of freedom. Like the GCM, the EGCM shows the sequence of freezing and remelting transitions, as well as the upper freezing temperature.

It follows from Eq. (4.15) that the free energy per particle depends on the combination $(\beta\Delta - \ln E)$. Note, however, that the entropy per particle depends explicitly on $\ln E$ and only implicitly on Δ (through the dependence of the equilibrium value of x_1 on Δ). Hence the occurrence of inverse melting in our model is determined primarily by the degeneracy E. For example, for $\sigma_{01}/\sigma_{00} = 0.98$, $\sigma_{11}/\sigma_{00} = 0.93$, $\Delta/\epsilon = 4$, a minimum value of $\ln E (\approx 30)$ is required to cause inverse melting across the entire range of temperatures (i.e., β) explored.

Figure 3 also shows the computed Kauzmann curves for the EGCM. These loci identify the supercooled liquid states that have the same entropy, pressure, and temperature as the crystal; and the overpressurized crystal states that have the same entropy, pressure and temperature as the liquid. In order to generate these Kauzmann curves for the EGCM, the Helmholtz free energies were numerically differentiated with respect to temperature at constant density. Note that two separate Kauzmann curves are shown in Fig. 3; one is cyclic and the other is not. The cyclic Kauzmann curve passes through both extrema (a,b) in the melting pressure-temperature curve. This intersection is consistent with the Calusius–Clapeyron Eq. (2.1) which states that for a nonzero volume of melting Δv an extremum in the melting pressure-temperature curve occurs in conjunction with a vanishing entropy of melting, Δs. The cyclic Kauzmann curve encloses the region in which the entropy of the thermodynamically stable solid is greater than that of the supercooled fluid, and the region in which the entropy of the overpressurized crystal is greater than that of the thermodynamically stable fluid. Note that the entire region of inverse melting lies within the cyclic Kauzmann curve.

A second Kauzmann curve exists at low temperature, and mirrors the solid–fluid equilibrium curve of the GCM. The latter Kauzmann curve encloses the region in which the thermodynamically stable crystal has a higher entropy than the supercooled fluid. Although we believe tentatively that the prediction of this noncyclic Kauzmann curve is realistic we also recognize that the HNC and Einstein approximations may be qualitatively unreliable in the $T \to 0$ limit. In order to remain consistent with the third law of thermodynamics, the entropy difference $\Delta s(T)$ that becomes negative upon passing the Kauzmann curve must in principle rise to zero or above in the $T \to 0$ limit.

Figure 5(a) shows the temperature dependence of the entropy difference between the supercooled fluid and the stable crystal at a reduced pressure of 0.411. This function has multiple zeros indicated by points I, II, and III. Figure 5(b) shows points I, II, and III in the pressure–temperature

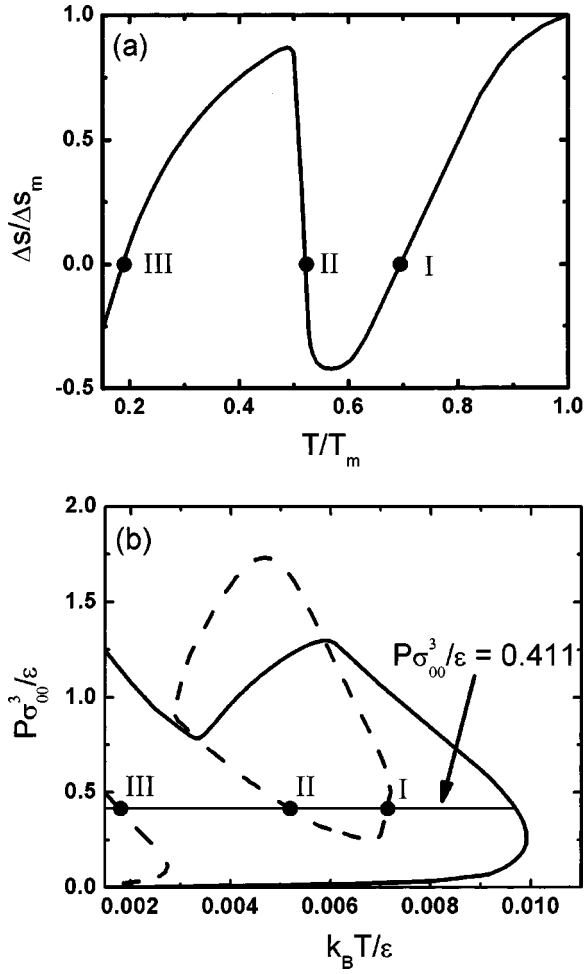

FIG. 5. (a) Isobaric temperature dependence of the entropy difference between the supercooled fluid and the stable crystal phase at $P^*=P\sigma_{00}^3/\epsilon=0.411$ for the EGCM with parameters as in Fig. 3. The function has multiple zeros shown by points I, II, and III. Δs_m is the melting entropy at the given pressure, and $T_m^*=k_BT_m/\epsilon$ is the melting temperature. The isobar of $P^*=0.411$ intersects the coexistence curve at the melting temperature $T_m^*=0.0097$. (b) Pressure–temperature projection of the calculated melting curve. Coexistence curves (solid lines), Kauzmann equal-entropy curves (dashed lines) and points I, II, and III, and the isobar at $P^*=0.411$ are shown.

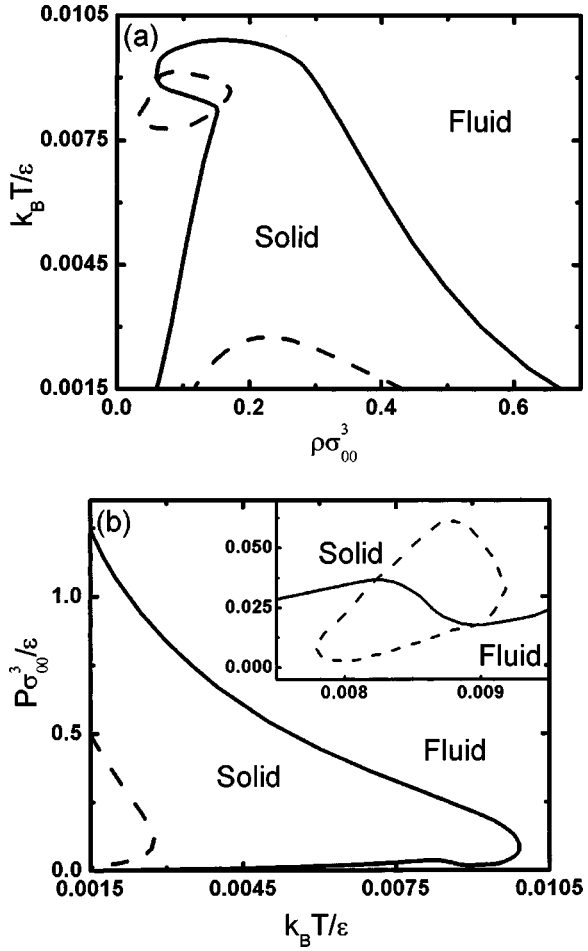

FIG. 6. Calculated phase behavior for the EGCM showing inverse melting on the low-pressure branch of the solid–liquid equilibrium curve. The model parameters are $\sigma_{00}/\sigma_{11}=0.70$, $\sigma_{01}/\sigma_{11}=0.81$, $\Delta/\epsilon=15$, and $E=\exp(200)$. Coexistence curves (dark solid) and Kauzmann equal-entropy curves (dashed lines) are shown. (a) Temperature–density projection. The density difference between the coexisting phases is too small to be visible on the scale of the figure. (b) Pressure–temperature projection. Solid–solid equilibrium lines are omitted for clarity. Calculations are shown for the more stable crystal phase at any given temperature and pressure.

projection of the calculated phase diagram. By definition these points must lie on Kauzmann curves. Starting at the melting temperature, $T/T_m=1$, initial cooling of the fluid results in the consumption of the entropy surplus. At point I the entropy of the solid is equal to that of the fluid. Between points I and II the entropy difference is negative. This corresponds to the region enclosed by the cyclic Kauzmann curve. A maximum in the entropy difference occurs between points II and III. At point III the entropy difference again vanishes. Beyond point III the entropy of the solid is greater than that of the fluid. However, in order to remain consistent with the third law of thermodynamics the entropy difference must eventually rise to zero or above in the $T\rightarrow 0$ limit, as discussed above.

The GCM was chosen as the basis for our study in part because it exhibits re-entrant melting, or a condition of vanishing melting volume Δv. This results in the possibility that the EGCM can predict inverse melting along the upper pressure branch, associated with a maximum on the melting pressure–temperature curve, or along the lower pressure branch, associated with a minimum on the melting pressure–temperature curve. We have shown in Fig. 3 that the EGCM is capable of the former case when internal excitation of a particle results in a decrease in σ ($\sigma_{11}<\sigma_{00}$). We will now describe the case in which σ grows upon excitation ($\sigma_{11}>\sigma_{00}$). Figure 6 shows solid–fluid equilibrium curves of the EGCM with $\sigma_{00}/\sigma_{11}=0.7$, $\sigma_{01}/\sigma_{11}=0.81$, $\Delta/\epsilon=15$, and $E=\exp(200)$. Once more the EGCM is capable of reproducing inverse melting. This time the anomalous region occurs along the lower-pressure branch, where the melting volume Δv is positive. As in the former example, the region of inverse melting is bounded by the extrema in the melting pressure–temperature curve. Figure 7 shows the fraction of excited fluid-phase particles $x_F=n_{1,F}/N$ along the freezing curve, as well as the difference between the excited fractions in the solid and fluid phases. The vertical line in Fig. 7(a) corresponds to the upper melting temperature T_u associated with the corresponding pressure P_u. Points to the left of the

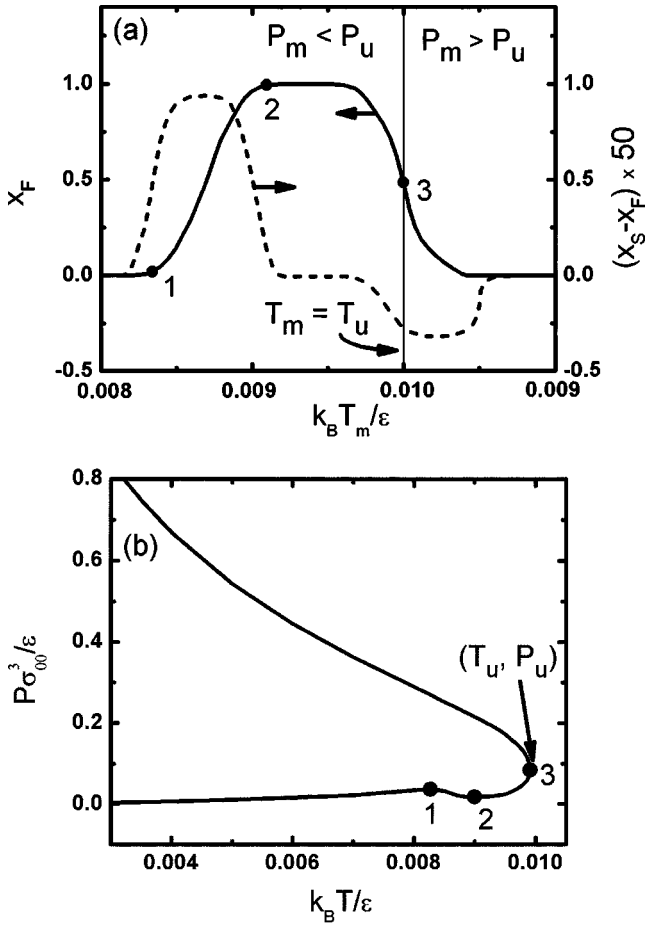

FIG. 7. (a) The fraction of excited particles in the fluid phase, x_F (solid line) and the difference between the fraction of excited particles in the solid and the fluid phases (dashed line) along the melting curve. The vertical line corresponds to the upper melting temperature, T_u; the values of melting temperature decrease to the right and left of this line (i.e., the melting curve is "unfolded" along the x-axis). Points to the left of the vertical line correspond to the lower pressure branch ($P_m < P_u$) and points to the right correspond to the upper pressure branch ($P_m > P_u$). Point 3 corresponds to the upper melting temperature T_u, at its corresponding pressure, P_u. Points 1 and 2 bound the region of inverse melting. EGCM parameters as in Fig. 6. (b) Pressure–temperature projection of the calculated melting curve.

vertical line correspond to the fraction of particles excited along the low-pressure branch ($P < P_u$) while points to the right of the vertical line correspond to the fraction of particles excited along the high-pressure branch ($P > P_u$). At low temperatures along the $P < P_u$ branch, virtually none of the particles in either phase are excited, $x_F \cong x_S \cong 0$. Points 1 and 2 bound the region of inverse melting. In this region, the fraction of particles that are excited increases as temperature rises, and the fraction of excited particles in the solid phase is greater than in the fluid phase, $x_S > x_F$. At the upper melting/freezing temperature, point 3, the fraction of excited particles has decreased considerably, and the fraction of excited particles in the solid phase lags behind that of the fluid phase, $x_S < x_F$. Following the coexistence curve to higher pressures reveals that essentially none of the particles are excited in the fluid or the solid phase, $x_F \cong x_S \cong 0$.

In addition to the solid–fluid equilibrium curve, two Kauzmann curves are shown in Fig. 6. The first is cyclic and passes through the two extrema in the melting pressure–temperature curve. It encloses the regions in which the thermodynamically stable solid has a higher entropy than the supercooled fluid, and the expanded crystal has a higher entropy than the thermodynamically stable fluid. The second Kauzmann curve occurs at low temperatures and is open. It is substantially identical to the low temperature Kauzmann curve shown in Fig. 3.

VII. CONCLUSIONS AND DISCUSSION

Inverse melting is an unusual type of phase behavior, in which a liquid freezes when it is heated isobarically. Accordingly, the crystal has a higher entropy than the liquid with which it coexists. A material exhibiting inverse melting can, in principle, be transformed into a glass by cooling the crystal at moderate rates. Thus, this phenomenon should be of interest in materials processing applications, such as the formation of amorphous alloys.[27] Both isotopes of helium exhibit inverse melting,[8,9] and published data suggests that the behavior may also occur in isotactic P4MP1.[10] In proteins, the often sharp transition between the biologically active, organized, native state, and the biologically inactive denatured forms provides a suggestive analogy to melting phenomena.[7] Interestingly, the denaturation locus of some proteins exhibits maxima in the (P,T) plane, of the type D in Fig. 1(b).[28,29] The possible existence of minima of the type B in Fig. 1(a) has also been discussed.[30] These examples suggest analogies and applications that warrant a deeper, microscopically-based understanding of inverse melting.

From a purely theoretical viewpoint too, inverse melting possesses considerable interest. Extrema in the melting curve, such as points A, B, C, and D in Fig. 1, are thermodynamic states where the entropy and enthalpy of the coexisting crystal and liquid phases are equal. The existence of such stable, experimentally accessible states, illustrates the logical disconnect between the vanishing of a liquid's configurational entropy and a condition of equal entropy between the liquid and crystal phases.[6] The former case has been suggested to correspond to structural arrest at an ideal glass transition,[31] and underlies, for example, the Adam–Gibbs theory of cooperative relaxation in supercooled liquids.[32] The latter condition, which we consider in this work, was originally thought of as a paradoxical situation in supercooled glassforming liquids,[33,34] which could, upon mild extrapolation, result in a potential conflict with the Third Law. This equal-entropy condition is now understood to pose no Third Law paradox, and carries no implication for relaxation behavior.[6]

Motivated by these examples, potential applications, suggestive analogies, and thermodynamic implications, we have proposed in this work a statistical mechanical model of inverse melting. Our starting point has been the Gaussian core model. This potential provides a reasonable representation of the effective, solvent-mediated interactions between polymer chains[13,17,18] and between colloidal particles.[19] Furthermore, this model exhibits expansion upon freezing, which can be thought of as a precursor of inverse melting [see Fig. 1(b)]. The model studied in this work is an internally decorated version of the Gaussian core model. Particles possess a spectrum of degenerate, thermally activated inter-

nal states. Excitation leads to a change in a particle's characteristic size, which in turn can result in a spatially periodic crystal having a higher entropy than the liquid with which it coexists. These internal degrees of freedom, in other words, can give rise to inverse melting.

When the above ideas are translated into statistical mechanical language, and reasonable simplifications are invoked to calculate the free energies of the solid and fluid phases, both types of inverse melting shown in Fig. 1 are obtained. Specifically, when the excited particles are sufficiently smaller than in their ground state, the behavior shown in Fig. 1(b), characteristic of P4MP1 and suggestive of proteins, is obtained. Conversely, when the excited particles are sufficiently larger than in their ground state, the behavior shown in Fig. 1(a), characteristic of both helium isotopes, is obtained. We believe that this is the first example of a classical statistical mechanical model capable of reproducing inverse melting.

Several directions for further study are suggested by this work. Alternative statistical mechanical approaches could include lattice models as well as a field-theoretic, Landau–Ginzburg formulation.[35] It is also possible to extend the present model to incorporate interchain entropic effects by replacing β in Eq. (4.9) by $(\beta-\beta^*)$, where β^* is a constant (with units of inverse energy), proportional to an entropic interchain contribution. Simulation studies aimed at verifying our theoretical calculations, and explicit treatment of segment–solvent interactions, such as would be needed to investigate the analogy with proteins, are also possible directions for extension of this work. Several of these lines of inquiry are being considered.

ACKNOWLEDGMENTS

P.G.D. gratefully acknowledges financial support by the U.S. Department of Energy, Division of Chemical Sciences, Geosciences, and Biosciences, Office of Basic Energy Sciences, Grant No. DE-FG02-87ER13714. M.R.F. gratefully acknowledges support from the National Science Foundation and American Association of University Women.

[1] A. R. Ubbelohde, *The Molten State of Matter: Melting and Crystal Structure* (Wiley, New York, 1978).
[2] W. G. Pfann, *Zone Melting*, 2nd ed. (Wiley, New York, 1966).
[3] P. G. Debenedetti, *Metastable Liquids: Concepts and Principles* (Princeton University Press, Princeton, 1996).
[4] A. Bar-Lev, *Semiconductor and Electronic Devices*, 3rd ed. (Prentice-Hall, New York, 1993).
[5] D. A. Young, *Phase Diagrams of the Elements* (University of California Press, Berkeley, 1991); D. Eisenberg and W. Kauzmann, *The Structure and Properties of Water* (Clarendon, Oxford, 1969).
[6] F. H. Stillinger, P. G. Debenedetti, and T. M. Truskett, J. Phys. Chem. B **105**, 11809 (2001).
[7] F. H. Stillinger and P. G. Debenedetti, Biophys. Chem. (to be published).
[8] E. R. Dobbs, *Helium Three* (Oxford University Press, Oxford, 2002).
[9] C. LePair, K. W. Taconis, R. DeBruyn Ouboter, and P. Das, Physica (Amsterdam) **29**, 775 (1963); J. Wilks, *The Properties of Liquid and Solid Helium* (Oxford University Press, Oxford, 1987).
[10] S. Rastogi, M. Newman, and A. Keller, Nature (London) **353**, 55 (1991); S. Rastogi, M. Newman, and A. Keller, J. Polym. Sci., Part B: Polym. Phys. **31**, 125 (1993); A. L. Greer, Nature (London) **404**, 134 (2000); S. Rastogi, G. W. H. Hohne, and A. Keller, Macromolecules **32**, 8897 (1999).
[11] F. H. Stillinger, J. Chem. Phys. **65**, 3968 (1976).
[12] F. H. Stillinger and D. K. Stillinger, Physica A **244**, 358 (1997).
[13] A. Lang, C. N. Likos, M. Watzlawek, and H. Lowen, J. Phys.: Condens. Matter **12**, 5087 (2000).
[14] A. A. Louis, P. G. Bolhuis, and J. P. Hansen, Phys. Rev. E **62**, 7961 (2000).
[15] H. Reiss, *Methods of Thermodynamics* (Dover, New York, 1996).
[16] A. B. Pippard, *The Elements of Classical Thermodynamics* (Cambridge University Press, Cambridge, 1957).
[17] P. J. Flory, *Principles of Polymer Chemistry* (Cornell University Press, Ithaca, 1953).
[18] C. N. Likos, M. Schmidt, H. Lowen, M. Ballauff, D. Potschke, and P. Lindner, Macromolecules **34**, 2914 (2001).
[19] A. A. Louis, P. G. Bolhuis, J. P. Hansen, and E. J. Meijer, Phys. Rev. Lett. **85**, 2522 (2000).
[20] F. H. Stillinger, Phys. Rev. B **20**, 299 (1979).
[21] F. H. Stillinger and T. A. Weber, J. Chem. Phys. **68**, 3837 (1978).
[22] M. Watzlawek, C. N. Likos, and H. Lowen, Phys. Rev. Lett. **82**, 5289 (1999); B. Groh and M. Schmidt, J. Chem. Phys. **114**, 5450 (2001); J. Bang, T. P. Lodge, X. Wang, K. L. Brinker, and W. R. Burghardt, Phys. Rev. Lett. **89**, 215505 (2002).
[23] A. J. Archer and R. Evans, Phys. Rev. E **64**, 041501 (2001); J. Chem. Phys. **118**, 9726 (2003).
[24] A. J. Archer and R. Evans, J. Phys.: Condens. Matter **14**, 113 (2002).
[25] J. P. Hansen and I. R. McDonald, *Theory of Simple Liquids*, 2nd ed. (Academic, New York, 1986).
[26] N. W. Ashcroft and N. D. Mermin, *Solid State Physics* (Holt Saunders, Philadelphia, 1976).
[27] A. L. Greer, J. Less-Common Met. **140**, 327 (1988).
[28] S. A. Hawley, Biochemistry **10**, 2436 (1971).
[29] J. Zhang, X. Peng, A. Jonas, and J. Jonas, Biochemistry **34**, 8361 (1995).
[30] L. Smeller, Biochim. Biophys. Acta **1595**, 11 (2002).
[31] F. H. Stillinger, J. Chem. Phys. **88**, 7818 (1988).
[32] G. Adam and J. H. Gibbs, J. Chem. Phys. **43**, 139 (1965).
[33] F. Z. Simon, Z. Anorg. Allg. Chem. **203**, 219 (1931).
[34] W. Kauzmann, Chem. Rev. **43**, 219 (1948).
[35] K. Huang, *Statistical Mechanics*, 2nd ed. (Wiley, New York, 1987).